In Situ Visualization of Paclitaxel Distribution and Release by Coherent Anti-Stokes Raman Scattering Microscopy

ARTICLE *in* ANALYTICAL CHEMISTRY · JANUARY 2007

Impact Factor: 5.64 · DOI: 10.1021/ac061218s · Source: PubMed

6 AUTHORS, INCLUDING:

Haifeng Wang
National University of Singapore
36 PUBLICATIONS **1,789** CITATIONS
SEE PROFILE

Il Keun Kwon
Kyung Hee University
106 PUBLICATIONS **3,097** CITATIONS
SEE PROFILE

Kinam Park
Purdue University
201 PUBLICATIONS **7,016** CITATIONS
SEE PROFILE

Ji-Xin Cheng
Purdue University
216 PUBLICATIONS **9,414** CITATIONS
SEE PROFILE

Anal. Chem. **2006,** *78,* 8036−8043

In Situ Visualization of Paclitaxel Distribution and Release by Coherent Anti-Stokes Raman Scattering Microscopy

Eunah Kang,[†] Haifeng Wang,[†] Il Keun Kwon,[‡] Joshua Robinson,[§] Kinam Park,[†,‡] and Ji-Xin Cheng*[,†,§]

Weldon School of Biomedical Engineering, Department of Pharmaceutics, and Department of Chemistry, Purdue University, West Lafayette, Indiana 47907

Visualization of three-dimensional distribution of drug molecules and subsequent changes during the release process is critical for understanding drug delivery mechanisms as well as designing tailor-made release profiles. This study utilized coherent anti-Stokes Raman scattering (CARS) imaging to examine paclitaxel distribution in various polymer films with lateral resolution of 0.3 μm and depth resolution of 0.9 μm. Raman bands in the CH stretch vibration and fingerprint regions were used to distinguish paclitaxel from the polymers. The detection sensitivity was measured to be 29 mM by imaging paclitaxel molecules dissolved in *N,N*-dimethylformamide solution. Release of paclitaxel from a polymer matrix was monitored at an acquisition speed of 1 frame/s. Our results show that CARS microscopy can be used effectively for in situ imaging of native drug molecules in a delivery system.

In many cases where a drug is directly released from a delivery device (e.g., a cardiovascular stent) to the surrounding target tissues, a very low dose can result in highly effective treatment. In such situations, careful control of the drug release kinetics is critical. Drug release from a controlled delivery system is normally characterized by chemical analysis of the solution containing the released drug molecules. Chemical analysis, however, does not provide the information about three-dimensional (3D) drug redistribution during the release process, which precludes in-depth understanding of the drug release mechanisms. Various chemical imaging methods including infrared (IR) microscopy,[1−4] Raman microscopy,[5−9] and secondary ion mass spectrometry[10,11] have been used to map drug distributions. While having molecular selectivity, IR microscopy suffers from strong IR absorption of water as well as poor spatial resolution of several micrometers due to its long excitation wavelength. Raman microscopy overcomes these problems owing to the weak Raman scattering from water and the shorter excitation wavelength used. Confocal Raman microscopy provides 3D spatial resolution.[12] However, the extremely small cross section of Raman scattering requires a long image acquisition time, usually tens of minutes to hours for a single frame. Secondary ion mass spectrometry provides good resolution and high sensitivity, but the measurement is invasive and usually restricted to thin films.

In this study, we demonstrate chemically selective imaging of native drug molecules using a nonlinear optical microscopy technique based on coherent anti-Stokes Raman scattering (CARS). In CARS microscopy,[13] a pump laser beam at frequency ω_p and a Stokes laser beam at frequency ω_s ($\omega_p > \omega_s$) are colinearly overlapped and tightly focused into a sample,[14] generating a signal field at the anti-Stokes frequency ($\omega_{as} = 2\omega_p - \omega_s$). The CARS signal is enhanced when $\omega_p - \omega_s$ is tuned to a Raman-active vibration, providing a chemically selective contrast. Because the signal is only generated inside the focal volume as two-photon fluorescence microscopy,[15] CARS microscopy as a nonlinear optical imaging method provides inherent 3D resolution and no further image processing is needed to produce depth-resolved images. Meanwhile, CARS microscopy possesses a significant advantage over fluorescence microscopy in that the CARS contrast arises from inherent molecular vibration. This capability is particularly attractive to imaging small drug molecules for which fluorophore labeling may significantly change the molecular properties. In contrast to the incoherent spontaneous Raman

* To whom correspondence should be addressed. Tel: 765-494-4335. Fax: 765-494-1193. E-mail: jcheng@purdue.edu.

[†] Weldon School of Biomedical Engineering.

[‡] Department of Pharmaceutics.

[§] Department of Chemistry.

(1) Kidder, L. H.; Kalasinsky, V. F.; Luke, J. L.; Levin, I. W.; Lewis, E. N. *Nat. Med.* **1997**, *3*, 235−237.

(2) Coutts-Lendon, C. A.; Wright, N. A.; Mieso, E. V.; Koenig, J. L. *J. Controlled Release* **2003**, *93*, 223−248.

(3) Kazarian, S. G.; Chan, K. L. A. *Macromolecules* **2003**, *36*, 9866−9872.

(4) Levin, I. W.; Bhargava, R. *Ann. Rev. Phys. Chem.* **2005**, *56*, 429−474.

(5) Breitenbach, J.; Schrof, W.; Neumann, J. *Pharm. Res.* **1999**, *16*, 1109−1113

(6) Feofanov, A. V.; Grichine, A. I.; Shitova, L. A.; Karmakova, T. A.; Yakubovskaya, R. I.; Egret-Charlier, M.; Vigny, P. *Biophys. J.* **2000**, *78*, 499−512.

(7) Schuster, K. C.; Reese, I.; Urlaub, E.; Gapes, J. R.; Lendl, B. *Anal. Chem.* **2000**, *72*, 5529−5534.

(8) Clarke, F. C.; Jamieson, M. J.; Clark, D. A.; Hammond, S. V.; Jee, R. D.; Moffat, A. C. *Anal. Chem.* **2001**, *73*, 2213−2220.

(9) Ling, J.; Weitman, S. D.; Miller, M. A.; Moore, R. V.; Bovik, A. C. *Appl. Opt.* **2002**, *41*, 6006−6017.

(10) Belu, A. M.; Davies, M. C.; Newton, J. M.; Patel, N. *Anal. Chem.* **2000**, *72*, 5625−5638.

(11) Mahoney, C. M.; Roberson, S. V.; Gillen, G. *Anal. Chem.* **2004**, *76*, 3199−3207.

(12) Sijtsema, N. M.; Wouters, S. D.; de Grauw, C. J.; Otto, C.; Greve, J. *Appl. Spectrosc.* **1998**, *52*, 348−355.

(13) Cheng, J. X.; Xie, X. S. *J. Phys. Chem. B* **2004**, *108*, 827−840.

(14) Zumbusch, A.; Holtom, G. R.; Xie, X. S. *Phys. Rev. Lett.* **1999**, *82*, 4142−4145.

(15) Helmchen, F.; Denk, W. *Nat. Methods* **2005**, *2*, 932−940.

10.1021/ac061218s CCC: $33.50
Published on Web 10/27/2006

scattering, the radiation fields from different molecules are in phase in a CARS process. Consequently, the coherent addition of CARS fields builds up a large and directional signal.[16] Moreover, the excitation energy in CARS can be focused on a single Raman band using picosecond pulses.[17] Recently, scanning of pulsed beams with high repetition rate lasers[18] has permitted high-speed image acquisition up to 20 frames/s.[19] CARS microscopy has been applied to lipid domains,[20,21] photoresists,[22] polymer films,[23] multilamellar systems,[24−26] live cells,[18,27,28] and live tissues.[19,29]

Paclitaxel (PTX) is one of the most widely used drugs in chemotherapy.[30−34] Delivery of paclitaxel (and sirolimus) from stents was shown to be highly effective in prevention of in-stent restenosis.[34−39] In the current work, CARS microscopy was applied to map PTX embedded in a variety of polymers currently used as stent coating materials for their known biocompatibility in vivo.[31,40] We present results about 3D distribution and in situ release of PTX from a polymer film coated on a glass. Our samples mimic the films coated on a drug eluting stent.

EXPERIMENTAL SECTION

Materials. Solvents of special reagent grade were purchased from Sigma-Aldrich, Inc. (Berkeley, CA). PTX (MW 854) was kindly supplied by Samyang, Ltd. (Seoul, Korea). Poly(2-hydroxyethyl methacrylate) (PHEMA; MW 3×10^5), poly(ethyl-*co*-vinyl acetate) (PEVA; 40 wt % vinyl acetate), and poly(butyl methacrylate) (PBMA; MW 3.4×10^5) were purchased from Aldrich, Inc. (Milwaukee, WI). Segmented polyurethane (PU; Cardiomat 610) was purchased from Polymer Technology Group, Inc. (Berkeley, CA). Poly(lactic-*co*-glycolic acid) (PLGA; equimolar lactic and glycolic acids, nominal inherent viscosity 0.59 dL/g, MW 4.4×10^4) was purchased from Birmingham Polymers, Inc. (Pelham, AL). PU was purified by precipitation in methanol. Other polymers and solvents were used as received.

Preparation of Films. A mixture of PEVA (or PHEMA, PLGA, PU, and PBMA) and PTX was dissolved in chloroform or tetrahydrofuran at a concentration of 15−20% w/v (or 150−200 mg/mL). The weight percentage of PTX in the PTX/polymer mixture was varied, ranging from 1 to 15 wt %, corresponding to 1.5−30 mg/mL PTX in the solution. Because PTX is soluble in both solvents at 70 mg/mL (unpublished results), there should be no PTX aggregation in our solutions. The solution was spin coated on a cleaned cover glass, with a thickness between 10 and 40 μm. After spin coating, films were dried under the vacuum overnight to remove the residual solvent prior to CARS imaging. To ensure that the solvent was thoroughly evaporated, we measured the weight changes of spin-coated films during the vacuum drying (1, 3, 6, 12, and 24 h). A total of four samples were tested for polyurethane in both solvents. After 1-h vacuum drying, the weight was slightly decreased (~5%), whereas after 3 h there was no change in weight. Therefore, the solvent can be completely removed from our film samples after 3 h vacuum drying.

CARS Imaging of PTX Distribution and Release. The CARS apparatus was reported previously.[8] Briefly, the pump and the Stokes beam were generated by two 2.5-ps Ti:sapphire oscillators (Mira 900, Coherent, Inc., Santa Clara, CA). Both lasers are tunable from 700 to 1000 nm, where water absorption is minimized. The two lasers were tightly synchronized (Sync-Lock, Coherent Inc.) with an average timing jitter of 100 fs. A Pockels cell was used to reduce the repetition rate from 76 to 1.3 MHz, which lowered the average power but maintained the high peak power at a sample. The laser beams were colinearly combined and directed into a confocal laser-scanning microscope (FV300/IX70, Olympus America Inc., Melville, NY). A 60× water immersion objective (NA = 1.2) was used to focus the excitation beams into the sample. The forward CARS (F-CARS) signal was collected by an air condenser (NA = 0.55) and detected with a photomultiplier tube (R3896, Hamamatsu). The acquisition speed was 1.12 s/frame. The pump and Stokes laser power at the sample was 1.0 and 0.4 mW, respectively. All the imaging experiments were conducted at room temperature of 22 °C.

For in situ observation of PTX release, a cover glass was coated with PTX-loaded PEVA film and attached to the frame of a petri dish to create an open chamber. The release medium was then added to the petri dish to cover the whole film. Because the glass transition temperature of PEVA ranges from −40 to −30 °C, well below room temperature, we expect the behavior of PTX release from the PEVA matrix at room temperature is close to that at 37 °C.

Raman and CARS Spectra. The Raman spectra of pure PTX and pure polymer films were recorded on a home-built portable Raman spectrometer. The excitation source is a 35-mW HeNe

(16) Cheng, J. X.; Volkmer, A.; Xie, X. S. *J. Opt. Soc. Am. B* **2002**, *19*, 1363−1375.
(17) Cheng, J. X.; Volkmer, A.; Book, L. D.; Xie, X. S. *J. Phys. Chem. B* **2001**, *105*, 1277−1280.
(18) Cheng, J. X.; Jia, Y. K.; Zheng, G.; Xie, X. S. *Biophys. J.* **2002**, *83*, 502−509.
(19) Evans, C. L.; Potma, E. O.; Puoris'haag, M.; Côté, D.; Lin, C. P.; Xie, S. *Proc. Natl. Acad. Sci. U.S.A.* **2005**, *102*, 16807−16812.
(20) Li, L.; Wang, H.; Cheng, J. X. *Biophys. J.* **2005**, *89*, 3480−3490.
(21) Potma, E. O.; Xie, X. S. *ChemPhysChem* **2005**, *6*, 77−79.
(22) Potma, E. O.; Xie, X. S.; Muntean, L.; Preusser, J.; Jones, D.; Ye, J.; Leone, S. R.; Hinsberg, W. D.; Schade, W. *J. Phys. Chem. B* **2004**, *108*, 1296−1301.
(23) Kee, T. W.; Cicerone, M. T. *Opt. Lett.* **2004**, *29*, 2701−2703.
(24) Müller, M.; Schins, J. M. *J. Phys. Chem. B* **2002**, *106*, 3715−3723.
(25) Cheng, J. X.; Pautot, S.; Weitz, D. A.; Xie, X. S. *Proc. Natl. Acad. Sci. U.S.A.* **2003**, *100*, 9826−9830.
(26) Kennedy, A. P.; Sutcliffe, J.; Cheng, J. X. *Langmuir* **2005**, *21*, 6478−6486.
(27) Potma, E. O.; de Boeij, W. P.; van Haastert, P. J. M.; Wiersma, D. A. *Proc. Natl. Acad. Sci. U.S.A.* **2001**, *98*, 1577−1582.
(28) Nan, X.; Cheng, J. X.; Xie, X. S. *J. Lipid Res.* **2003**, *40*, 2202−2208.
(29) Wang, H.; Fu, Y.; Zickmund, P.; Shi, R.; Cheng, J. X. *Biophys. J.* **2005**, *89*, 581−591.
(30) McGuire, W. P.. Rowinsky, E. K., Eds. *Paclitaxel in cancer treatment*; Marcel Dekker: Inc.: New York, 1995.
(31) Stone, G. W.; Ellis, S. G.; Cox, D. A.; Hermiller, J.; O'Shaughnessy, C.; Mann, J. T.; Turco, M.; Caputo, R.; Bergin, P.; Greenberg, J.; Popma, J. J.; Russell, M. E. *N. Engl. J. Med.* **2004**, *350*, 221−231.
(32) Koziara, J. M.; Whisman, T. R.; Tseng, M. T.; Mumper, R. J. *J. Controlled Release* **2006**, *112*, 312−319.
(33) Park, E. K.; Kim, S. Y.; Lee, S. B.; Lee, Y. M. *J. Controlled Release* **2005**, *109*, 158−168.
(34) Westedt, U.; Wittmar, M.; Hellwig, M.; Hanefeld, P.; Greiner, A.; Schaper, A. K.; Kissel, T. *J. Controlled Release* **2006**, *111*, 235−246.
(35) Degertekin, M.; Serruys, P. W.; Foley, D. P.; Tanabe, K.; Regar, E.; Vos, J.; Smits, P. C.; van der Giessen, W. J.; van den Brand, M.; de Feyter, P.; Popma, J. J. *Circulation* **2002**, *106*, 1610−1613.
(36) Grube, E.; Büllesfeld, L. *J. Interv. Cardiol.* **2002**, *15*, 471−475.
(37) Grube, E.; Silber, S.; Hauptmann, K. E.; Mueller, R.; Buellesfeld, L.; Gerckens, U.; Russell, M. E. *Circulation* **2003**, *107*, 38−42.
(38) Sousa, J. M.; Costa, M. A.; Abizaid, A. C.; Sousa, A. G.; Feres, F.; Mattos, L. A.; Centemero, M.; Maldonado, G.; Abizaid, A. S.; Pinto, I.; Falotico, R.; Jaeger, J.; Popma, J. J.; Serruys, P. W. *Circulation* **2003**, *107*, 24−27.
(39) Chen, M.-C.; Liang, H.-F.; Chiu, Y.-L.; Chang, Y.; Wei, H.-J.; Sung, H.-W. *J. Controlled Release* **2005**, *108*, 178−189.
(40) Giessen, V. d. *Circulation* **1996**, *94*, 1690.

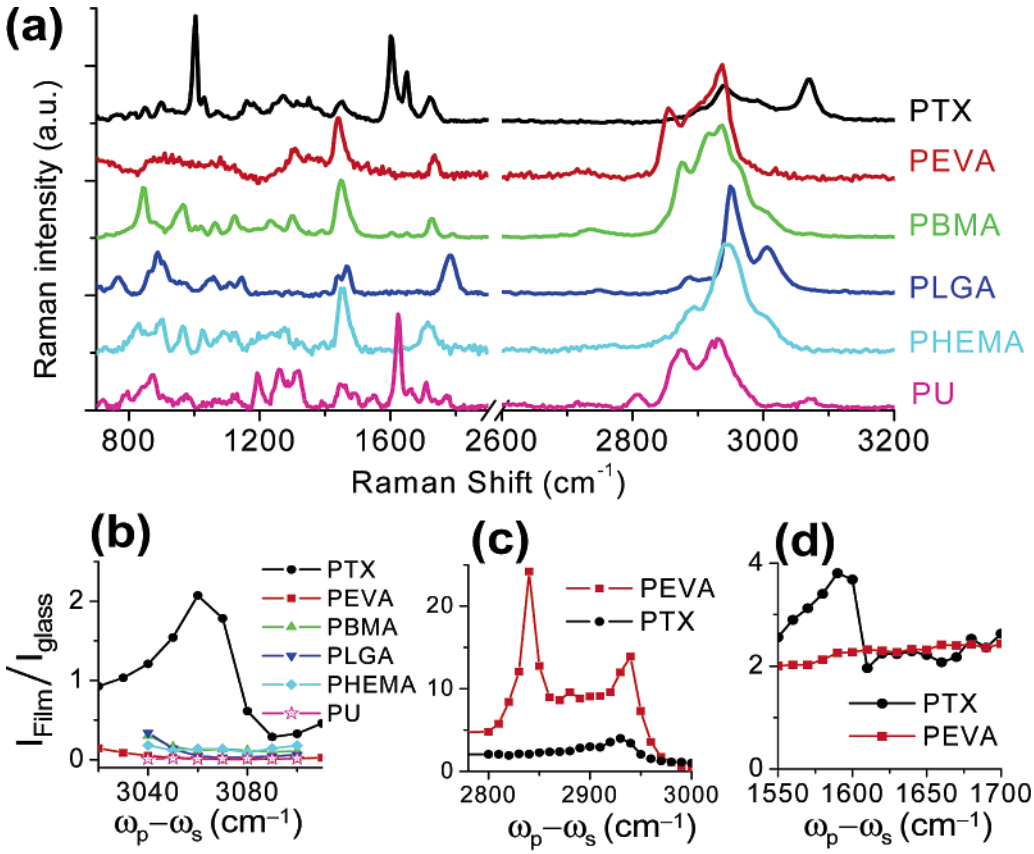

Figure 1. Raman and CARS spectra of PTX and polymers. (a) Raman spectra of PTX, PEVA, PBMA, PU, PHEMA, and PLGA. (b) CARS spectra of PTX, PEVA, PBMA, PU, PHEMA, and PLGA in the region of 3020−3120 cm^{-1}. (c) CARS spectra of PTX and PEVA in the region of 2800−3000 cm^{-1}. (d) CARS spectra of PTX and PEVA in the region of 1550−1700 cm^{-1}.

laser at the wavelength of 632.8 nm. The CARS spectra of the same film samples were obtained by manually tuning the Stokes frequency. The CARS signal from the sample was normalized by the nonresonant CARS signal from glass to remove the signal fluctuation induced by the variation in laser power and detector efficiency.

RESULTS AND DISCUSSION

Raman and CARS Spectra of PTX and Polymers. The Raman spectra of spin-coated films of pure PTX and each polymer were recorded to determine the vibrational bands for selective imaging of PTX and the polymers including PEVA, PBMA, PHEMA, PLGA, and PU. The results are shown in Figure 1a. The phenyl groups in PTX contributed to a strong aromatic CH stretch vibration band centered at 3070 cm^{-1}. None of the polymers have aromatic CH except PU, which shows a small peak at 3070 cm^{-1}. Thus, the aromatic CH band was used to image PTX in these polymer films. All the polymers displayed a strong CH_2 stretch vibration band at 2850 cm^{-1}, a strong CH_3 stretch vibration band at 2940 cm^{-1}, or both. Moreover, these two bands were much stronger for the polymers than for PTX and they were used for imaging the polymer matrices.

The CARS signal is a coherent addition of a nonresonant and a resonant field.[41] Due to the interference between these two fields, the CARS spectra have line shape and peak positions different from the Raman spectra of the same sample.[41] Therefore, we also recorded the CARS spectra of PTX and each of the polymers by manually tuning the Stokes laser frequency. In the 3020−3120 cm^{-1} region (Figure 1b); the CARS spectrum of PTX displayed a peak at 3060 cm^{-1} and a dip at 3090 cm^{-1}. In contrast, all the polymers had negligible CARS signals in this region because of the destructive interference between the C−H vibrations and the nonresonant contribution. Therefore, the aromatic CH band was used for selective imaging of PTX.

The polymers gave a strong CARS signal from either CH_2 or CH_3 stretch vibration. As shown in Figure 1c, the CARS spectrum of a PEVA film displayed a strong peak at 2840 cm^{-1}, contributed by the symmetric CH_2 stretch vibration, and a medium strong peak at 2940 cm^{-1}, contributed by the CH_3 stretch vibration. Figure 1c also indicates that the CARS signal at 2840 cm^{-1} from a film of pure PTX is 10 times smaller than that from a film of pure PEVA. As a result, for a PEVA/PTX film, the morphology of the PEVA matrix can be represented by the CARS image taken at 2840 cm^{-1}. This method is applicable to other polymers except PLGA for which the stronger CH_3 vibration peak at 2940 cm^{-1} is used.

Although the aromatic CH stretch vibration band allowed us to distinguish PTX from the polymers, it was not suitable for imaging PTX in an aqueous environment due to the broad CARS band of OH stretch vibration.[26] We found that water generates a considerable CARS signal at 3060 cm^{-1} and an even larger signal at 3090 cm^{-1} due to vibrational enhancement. The water signal

(41) Shen, Y. R. *The principles of nonlinear optics*; John Wiley and Sons Inc.: New York, 1984.

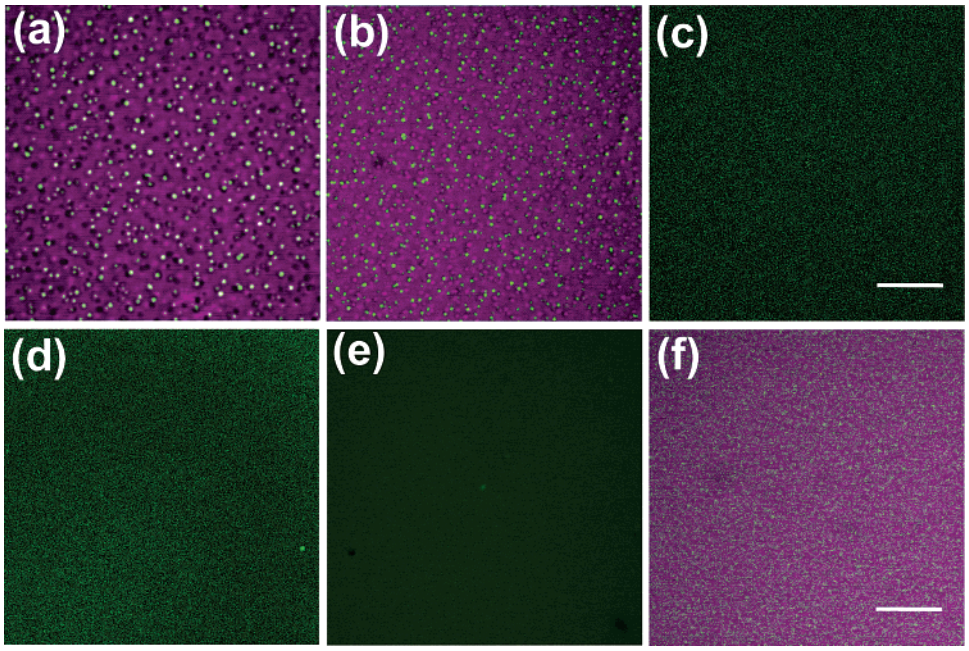

Figure 2. PTX distribution in various polymer films. (a) Overlaid CARS images of PEVA (magenta) and PTX (green) in a PEVA/7.5% PTX film. (b) Overlaid CARS images of PBMA (magenta) and PTX (green) in a PBMA/7.5% PTX film. (c) CARS image of PTX (green) in a PLGA/15% PTX film. (d) CARS image of PTX (green) in a PHEMA/15% PTX film. (e) CARS image of PTX (green) in a PU/15% PTX film. (f) Overlaid CARS images of PEVA (magenta) and PTX (green) in a PEVA/7.5% PTX film labeled with 0.075% OG−PTX. For all images, the distribution of PTX is obtained by subtracting the image at 3090 cm^{-1} from the one at 3060 cm^{-1}. The acquisition time for each image was 1.12 s. Bar, 10 μm.

partially canceled out the contrast from PTX, complicating the interpretation of data. To avoid this difficulty, we examined the CARS spectra of PTX and PEVA in the 1550−1700 cm^{-1} region (Figure 1d). There we observed a peak at 1590 cm^{-1} and a dip at 1610 cm^{-1} from PTX, contributed by the C=C stretch vibration, and purely nonresonant contributions from PEVA. It was also observed that pure water generated a nonresonant background in this region.[17] Therefore, the C=C band can be used for imaging PTX distribution inside a PEVA film in an aqueous environment.

PTX Distribution in Different Polymers. Using CARS microscopy, we have examined the dispersion as well as coagulation of PTX in various solid polymer matrixes. Figure 2a is a CARS image taken at the mid-depth of a PEVA/7.5% PTX film. The morphology of the polymer matrix was not uniform due to the existence of PTX particles. Further polarization analysis showed these particles were not in the crystalline form. Phase separation of PTX also occurred in the PBMA/7.5% PTX film (Figure 2b), but the PTX particles were smaller than those in Figure 2a. No remarkable PTX particles were observed in the PLGA/15% PTX (Figure 2c), PHEMA/15% PTX (Figure 2d), and PU/15% PTX (Figure 2e) films.

Because the amount of PTX in our solutions was far below the saturating solubility, we attribute the formation of PTX particles in the PEVA and PBMA films to aggregation of PTX during the fast evaporation process. The mechanism for drug dispersion in a solid polymer matrix was postulated to be relevant to the extent of interactions between drug and polymer molecules.[42,43] As a simplified analysis, we evaluated the drug−polymer compatibility by calculating the Flory−Huggins interaction parameter: $\chi = (\delta_d - \delta_p)^2 V_d/RT$, where δ_d and δ_p are the Hildebrand solubility parameters of the drug and the polymer, respectively. V_d is the molar volume of the drug. R is the gas constant, and T is the Kelvin temperature. The highest solubility is reached when $\delta_d = \delta_p$. Using the method of Hoftyzer and van Krevelen,[44] the solubility parameters were calculated to be 18.56, 19.07, 25.08, 27.11, 21.26, and 26.97 for PEVA, PBMA, PU, PHEMA, PLGA, and PTX, respectively. These calculations roughly explain our observation. For instance, PEVA has the lowest solubility parameter, which accounts for the largest PTX particles in the PEVA film.

To examine the possible perturbation of PTX distribution by fluorophore labeling, a film containing PEVA, 7.5% PTX, and 0.075% Oregon Green-conjugated PTX (OG−PTX) were prepared under the same condition. A CARS image focused at the mid-depth of the film was shown in Figure 2f. It is clear that incorporation of 0.075% OG−PTX led to much smaller PTX aggregations compared to the PTX particles in the unlabeled film (Figure 2a), probably due to the conjugation of Oregon Green. This result confirms the significance of imaging small drug molecules in their natural form.

In the above experiments, the different vibrational frequencies of aromatic and aliphatic C−H groups were utilized to selectively image PTX and polymers. The aromatic C−H band, however, was not suitable for imaging samples in an aqueous solution due to the perturbation by the OH vibration from H_2O. In such cases, the fingerprint Raman bands were more appealing because they were more specific and away from CH, NH, and OH stretch vibrations. For films covered with an aqueous solution, PTX

(42) Sekikawa, H.; Nakano, M.; Arita, T. *Chem. Pharm. Bull.* **1978**, *26*, 118−126.
(43) Li, J.; Masso, J. J.; Rendon, S. *J. Controlled Release* **2002**, *82*, 1−16.
(44) Brandrup, J., Immergut, E. H., Grulke, E. A., Abe, A., Bloch, D. R., Eds. *Polymer Handbook*; John Wiley & Sons: New York, 1999.

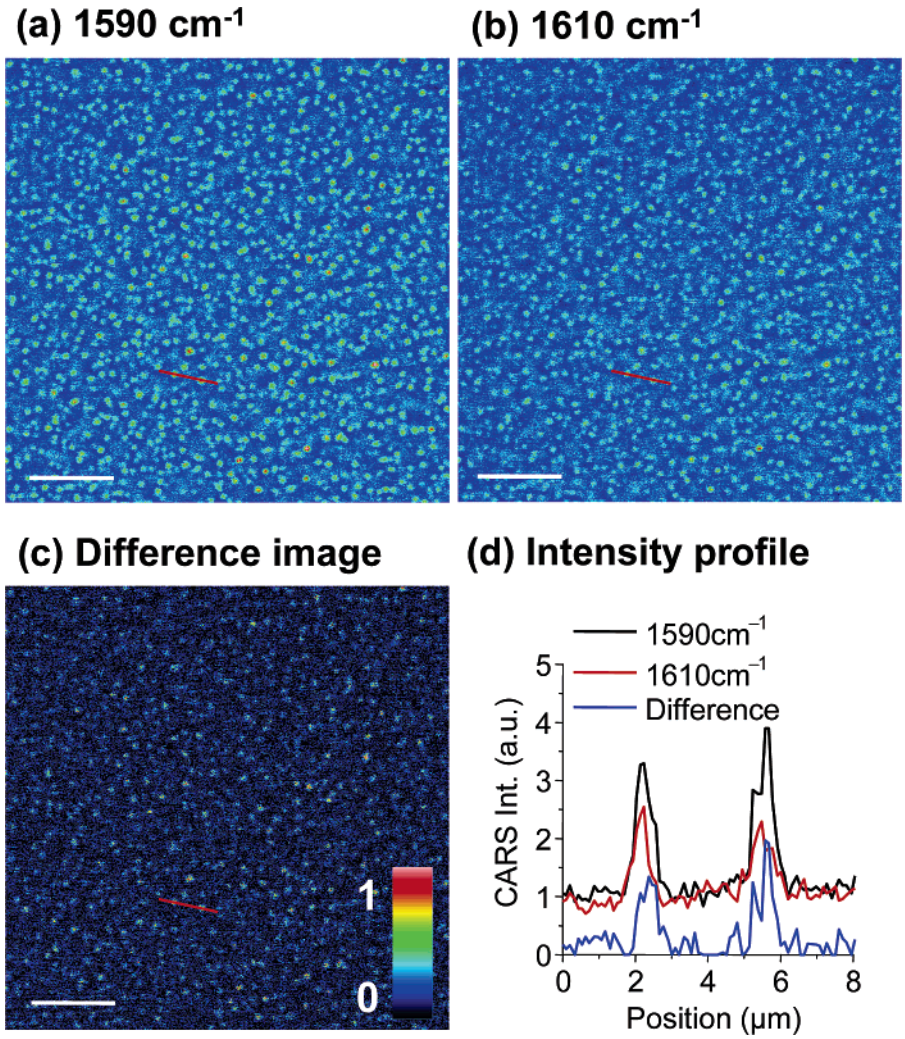

Figure 3. Imaging PTX with a fingerprint Raman band. Spectrum color scheme was used to emphasize the change of contrast. (a, b) CARS images taken at 1590 and 1610 cm^{-1}, respectively. (c) Difference image obtained by subtracting (b) from (a). (d) CARS intensity profiles along the red lines in (a−c). Bar, 10 μm.

distribution using the C=C stretch vibration band was examined. For this Raman band, the spectral profiles shown in Figure 1d indicate that the vibrational contrast is compromised by the nonresonant CARS background contributed by both PTX and PEVA. In this case, we acquired CARS images of a PEVA/7.5% PTX film at 1590 (near peak) and 1610 cm^{-1} (near dip). The images were taken from the same position at the mid-depth of the film. The distribution of PTX was derived by subtracting the image taken at 1610 cm^{-1} from that taken at 1590 cm^{-1}. As shown in Figure 3c, PTX exists in the form of particles, consistent with Figure 2a obtained with the aromatic CH stretch band. The nonresonant background from the PEVA matrix is completely removed in the difference image, as one can see from the intensity profiles along the red lines (Figure 3d).

With near-IR excitation wavelengths, the detection depth of CARS is between 100 and 300 μm depending on the sample properties.[19,29] This value is much larger than the thickness of most films on stents or particulate drug delivery systems. The penetration capability and 3D resolution of CARS microscopy allow us to analyze the depth distribution of PTX. We have recorded 3D images of PEVA films containing 5, 1, and 0% PTX. The lateral distribution of PTX was found uniform in the 5% and 1% films. The Z profiles of PTX were obtained from the integrated CARS intensities for each depth measured at the peak (3060 cm^{-1}) and the dip (3090 cm^{-1}) of the aromatic CH band. The results are shown in Figure 4. For the film containing 0% PTX, the CARS signals at 3060 and 3090 cm^{-1} had mean values of 17.3 and 17.8 au, with a standard deviation of 3.5 au, indicating no difference between 3060 and 3090 cm^{-1}. For the film containing 1% PTX, the CARS signals at 3060 and 3090 cm^{-1} had mean values of 16.2 and 9.7 au, with standard deviation of 1.1 au. These measurements demonstrate that our setup is able to probe 1% PTX in the polymer films. Because the concentration of PTX embedded in a polymer film on a stent is usually between 8 and 35%,[45] our method is qualified to follow PTX release from a polymer matrix.

To characterize the depth distribution of PTX in the polymer film, we also measured the depth profile at 2840 cm^{-1} (CH_2 peak for PEVA) for the same samples. Combining the depth profiles for polymer and PTX, we observed a larger PTX signal in the upper layer of the films, especially for the 1% PTX sample. For the pure polymer film, the polymer CARS signal was uniform inside the film. However, for the films containing PTX, the polymer

(45) Ranade, S. V.; Miller, K. M.; Richard, R. E.; Chan, A. K.; Allen, M. J.; Helmus, M. N. *J. Biomed. Mater. Res. Part A* **2004**, *71A*, 625−634.

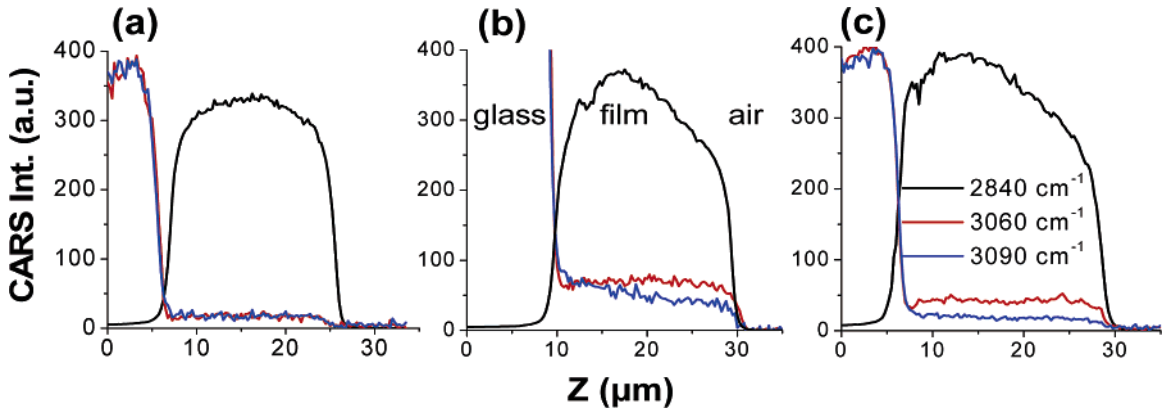

Figure 4. Depth (Z) distribution profile of PTX in a PEVA film. (a) PEVA film containing 0% PTX. (b) PEVA film containing 1% PTX. (c) PEVA film containing 5% PTX. The black, red, and blue lines represent the CARS intensities obtained at 2840, 3060, and 3090 cm^{-1}, respectively. The region of the film is defined by the CARS signal at 2840 cm^{-1}. Below the film was the cover glass, which generated a large nonresonant CARS signal. Above the film was air, and the CARS signal was zero. For the film containing 1% PTX, the CARS intensities at 3060 and 3090 cm^{-1} are magnified by 5 times.

CARS signal from the top of the film was lower by 30% than that from the bottom of the film. This signal reduction was likely caused by Rayleigh scattering of excitation beams by the PTX particles inside the film. For films containing sizable PTX particles (e.g., the 7.5% PTX/PEVA film shown in Figure 2a), the CARS signal could be significantly reduced inside a 3D sample. Therefore, calibration of CARS intensity attenuation along the depth is needed for quantitative analysis of depth distribution.

We note that the CARS contrast for 5% PTX was found to be 5 times of that from 1% PTX. This linear relationship is explained as follows. The CARS signal arises from the third-order susceptibility,[41] $\chi^{(3)}(\delta) = N(A/(\delta - i\Gamma)) + \chi_{nr}$, where $\delta = \Omega - (\omega_p - \omega_s)$ is the detuning, Ω is the vibrational frequency, represents the full width at half-maximum (FWHM) of the Raman band, N is the number of Raman oscillators, A is the strength of the Raman band, and χ_{nr} is the nonresonant susceptibility contributed by both PTX and polymer. For an isolated Raman band such as the aromatic CH vibration in PTX, the CARS intensity I is proportional to the square amplitude of $\chi^{(3)}(\delta)$ and can be written as

$$I = \eta\left(\frac{N^2A^2}{\delta^2 + \Gamma^2} + \chi_{nr}{}^2 + \frac{2N\chi_{nr}A}{\delta^2 + \Gamma^2}\delta\right) \qquad (1)$$

where η is a factor related to detector efficiency and excitation intensities. The first and second terms in eq 1 represent the resonant signal and nonresonant background, respectively. The third term is the interference term, which accounts for the dispersive profile of a CARS band.[41] At low molecular concentrations, the difference of the CARS intensities measured at the peak and the dip of a CARS band is mainly contributed by the interference term and is linear with respect to the number of molecular oscillators (N). Such linear relationship has been found in CARS measurement of lipid in a single bilayer[20] and methanol in water.[46]

Spatial Resolution and Sensitivity. The lateral and depth resolution of laser-scanning CARS microscopy with a 60× water immersion objective was measured to be 0.23 and 0.75 μm based on the XY CARS image of 0.1-μm polystyrene beads and the XZ CARS image of 0.2-μm polystyrene beads, respectively.[18] Considering that the polymer sample may affect the focusing and thus the spatial resolution, we measured the lateral and depth resolution from the FWHM of the depth intensity profile across the PTX

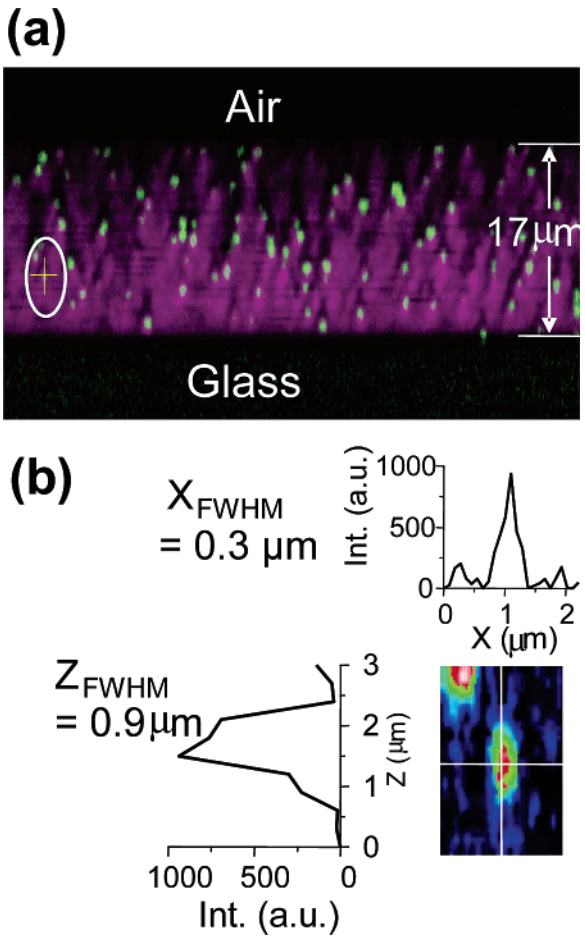

Figure 5. Characterization of spatial resolution. (a) Depth image of PTX (green) in a PEVA film (magenta). (b) Digitally magnified image of a PTX particle shown in (a). The intensity profiles of the PTX particle along the X and Z axes are shown above and on the left of the image.

(46) Ganikhanov, F.; Evans, C. L.; Saar, B. G.; Xie, X. S. *Opt. Lett.* **2006**, *31*, 1872−1874.

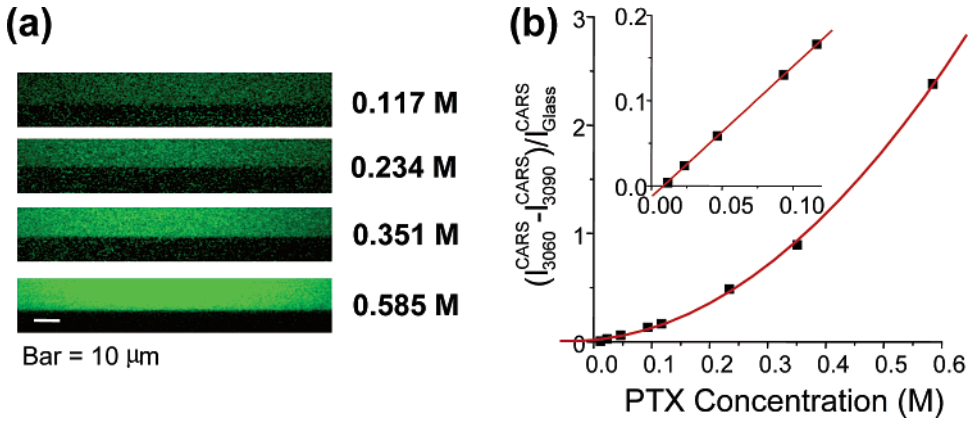

Figure 6. Characterization of PTX detection sensitivity. (a) Difference CARS image of PTX dissolved in DMF at marked molar concentrations. (b) The measured PTX signal (squares) as a function of PTX concentration. The PTX signal is normalized by the glass signal. The red curve represents least-squares fitting by $y = 0.015 + 0.50x + 6.03x^2$, with x and y being the PTX concentration and the difference CARS intensity. The inset shows the linear relationship between the CARS signal and PTX concentration at the low concentration region.

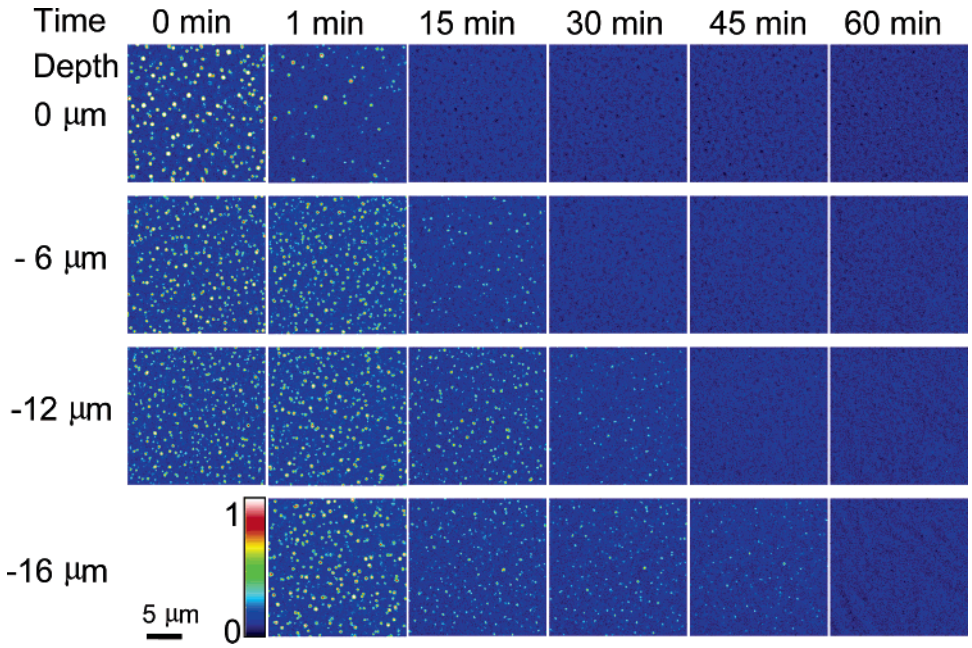

Figure 7. In situ CARS imaging of PTX release from a PEVA film. Spectrum color scheme was used to emphasize the change of contrast. The columns were arrayed as time lapse, and the rows were arrayed as depth of the film. The CARS images were taken from different depths of the film with $\omega_p - \omega_s$ tuned to 3060 cm^{-1}. The acquisition time for each image was 1.12 s.

particle dispersed in PEVA film (Figure 5b): The lateral resolution was 0.3 μm, and the depth resolution was 0.9 μm.

We acquired *XZ* CARS images of a PEVA/PTX (7.5% in weight) film, with the *X* axis parallel to the film surface and the *Z* axis perpendicular to it. Two CARS images at 3090 (peak) and 3090 cm^{-1} (dip) were acquired. The 3090 cm^{-1} image was then subtracted from the 3060 cm^{-1} image to remove the nonresonant background. The resultant difference image displayed purely vibrational contrast contributed by PTX. Figure 5a shows the overlay of the image of PEVA taken at 2840 cm^{-1} (in magenta) and the difference (3060 − 3090 cm^{-1}) image of PTX (in green). In accordance with Figure 5a, PTX was observed to form particles. The circled part of the image containing a small PTX particle was magnified and shown in Figure 5b. The FWHM of the lateral and axial intensity profiles across the PTX particle are 0.3 and 0.9 μm, respectively, corresponding to an excitation volume of 0.063 μm^3. These values are close to the spatial resolution previously measured with polystyrene beads.[18]

To quantify the PTX detection sensitivity, PTX was dissolved in *N,N*-dimethylformamide (DMF) at various concentrations. DMF was chosen for its high PTX solubility (over 100 mg/mL, unpublished result) and extremely low solvent evaporation, which ensures the accuracy of the PTX concentration. The solution was then placed in a chamber with a cover glass bottom. *XZ* CARS images of the PTX solution above a cover glass are shown in Figure 6a. The images were acquired by subtracting the CARS intensity at 3090 cm^{-1} from that at 3060 cm^{-1}. Because the glass generates only nonresonant CARS, the glass region located at the bottom half of each image shows a dark contrast. The bursts in the glass region are contributed by the electronic noise. The difference of the CARS intensities between 3060 and 3090 cm^{-1} (ΔI_{CARS}) measured from the solution was normalized by the

nonresonant signal from glass. The normalized signal was plotted against the PTX concentration (Figure 6b). The inset of Figure 6b shows that ΔI_{CARS} is linear to the PTX concentration lower than 0.15 M, where ΔI_{CARS} is mainly contributed by the interference term (the third term in eq 1). At higher PTX concentrations, ΔI_{CARS} is dominated by the resonant CARS signal (the first term in eq 1) and thus increases quadratically with the PTX concentration. We were able to detect PTX at a concentration as low as 29 mM, corresponding to 1.8 amol (10^{-18} mol) per focal volume of 0.063 μm^3.

In Situ PTX Release. To demonstrate the ability of CARS microscopy to monitor drug release in situ, we studied the release of PTX from a PEVA/7.5% PTX film in a phosphate-buffered saline (PBS) medium prepared with D_2O. The PBS medium was supplemented with 50% isopropyl alcohol, which serves as a sink of PTX. Because the nonresonant background from the polymer is negligible in the 3020−3100-cm^{-1} region (Figure 1b), CARS images at 3060 cm^{-1} taken from different depths of the film were directly used to follow the 3D PTX release over time. The time- and depth-resolved CARS images are shown in Figure 7. Before the release experiment began, PTX existed as particles in the sample (first column). In 1.0 min, the number of particles significantly reduced and pores (dark holes in the image) started to appear at the film surface (second column). After 15 min of release, all the particles were removed from the surface and pores were observed in the middle of the film (third column). After 60 min, all the PTX particles were released from the film. Interestingly, the pattern of the pores on the film surface was not changed during the whole process, suggesting that PTX inside the film is released through the pores created in the upper layers.

CONCLUSIONS

We have shown that CARS microscopy can be used effectively for imaging native drug molecules in polymer matrixes. The advantages of this technique are as follows: no need for labeling, noninvasiveness to the sample, high detection sensitivity, real-time imaging capability, and 3D spatial resolution. For most drug delivery systems such as the drug-eluting stents, CARS bands that are unique for drugs and polymers can be easily identified, as shown in this study. CARS microscopy can be used to determine the optimal amount of a given agent to be administrated and will help rational design of controlled drug delivery system. This new tool is expected to find various applications for research in the pharmaceutical and biomedical fields.

ACKNOWLEDGMENT

This work is supported by NIH through grants HL78715 and EB004906. The authors thank Dr. Jian Lian for a critical reading of the manuscript. E.K. and H.W. contributed equally to this work.

Received for review July 5, 2006. Accepted September 18, 2006.

AC061218S